On the origin of surface ozone episode in Shanghai over Yangtze River Delta during a prolonged heat wave

Jian-Bin Wu[1,4,*], Qian Wang[2], Huansheng Chen[1,*], Yuqia Zhang[1], Oliver Wild[3]

[1] *State Key Laboratory of Atmospheric Boundary Layer Physics and Atmospheric Chemistry,*

Institute of Atmospheric Physics, Chinese Academy of Sciences, Beijing 100029, China

[2] *Shanghai Environmental Monitoring Center, Shanghai 200235, China*

[3] *Lancaster Environment Centre, Lancaster University, Lancaster LA1 4YQ, UK*

[4] *Shanghai Key Laboratory of Meteorology and Health, Shanghai, 200135, China*

Abstract

A heat wave with temperatures over 35°C and sunny stagnant meteorological conditions occurred in Shanghai from 27 July to 5 August 2015, leading to a sustained episode of high ozone lasting 12 days. We have conducted a detailed source apportionment of surface ozone, by precursor source category and region, using a photochemical transport model. In this episode, a southwesterly wind prevailed over the Yangtze River Delta, and therefore precursors from the local Shanghai region and the region immediately to the south of Shanghai are the two major contributors (in total 90%) to ozone in Shanghai. The source apportionment reveals that local industrial sources and energy/biogenic sources in neighbouring regions are the principal causes for the high levels of ozone. By examining the contributions from individual physical and chemical processes, we show that ozone concentrations start to rise rapidly in the morning because chemical production dominates as the solar radiation increases, and while there is little removal by deposition when ozone remains low. In general, chemical production, horizontal advection and vertical diffusion contribute to increase ozone concentration during daytime, and deposition and vertical advection reduce ozone concentrations.

Keywords: Ozone; Source apportionment; Process analysis; Heat wave; Shanghai.

[1]

---

* Corresponding author.

E-*mail address*: Huansheng Chen (chenhuansheng@mail.iap.ac.cn), Jian-Bin Wu (wujianbin83@126.com)

INTRODUCTION

High ozone (O_3) episodes are one of the most severe air pollution issues experienced in megacities (Wild et al. 2004; Shao et al., 2006; Streets et al., 2007; Yang et al., 2008; Zhang et al. 2008). Severe O_3 pollution events in troposphere can cause adverse effects on human health, crop productivity and ecosystems (Feng et al., 2003; Fann and Risley, 2013; Landry et al., 2013). In recent years, the O_3 concentrations exceeding moderately polluted level (the daily maximum 8-h moving average O_3 concentration >100 ppbv defined by the National Ambient Air Quality Standard of China) have been frequently observed in China (Wang et al., 2001, 2009; Wang et al., 2006a; Ding et al., 2008, 2013; Xu et al., 2008; Tang et al., 2009; Shao et al., 2009; Ran et al., 2009).

O_3 concentrations are affected by chemical formation and loss related to local precursors emissions, and by transport of O_3 and its precursors from other regions. For chemical formation, O_3 is a secondary pollutant formed nonlinearly by chemical reactions involving nitrogen oxides (NO_x) and volatile organic compounds (VOCs) in the presence of solar radiation (Crutzen et al., 1999; Kumar et al., 2008). High O_3 concentrations are also affected by favorable weather conditions, such as extremely high temperature, strong solar radiation, low relative humidity and weak wind speed (Shu et al., 2016). These weather conditions are usually accompanied by strong subtropical high, and play a crucial role in transport, accumulation and fast chemical production

50   of O_3 in the boundary layer. Shanghai as well as surrounding city cluster (namely as Yangtze

51   River Delta, YRD), locate on the eastern coast of China, and are generally affected by the

52   western Pacific subtropical high in summertime. Therefore, high-level O_3 events are observed in

53   summertime with relationship to synoptic systems (Huang et al., 2006; Jiang et al., 2012; Ding et

54   al., 2013; Xie et al., 2016).

55   O_3 pollutions in the YRD have been previously analyzed (Wang et al., 2006b; Geng et al.,

56   2008; Ran et al., 2009; Jiang et al., 2012), but some properties controlling O_3 behavior in this area

57   remain uncertain, especially during a typical weather system in this region. Effective attainment

58   of ground-level O_3 concentration depends upon a reliable understanding of how O_3 responds to

59   control of its precursors (Cohan et al., 2007). In this study, we apply the Comprehensive Air

60   Quality Model with Extensions model (CAMx) to study the typical weather system and the exact

61   formation mechanism of the O_3 pollution over YRD region. A better understanding of O_3

62   source-receptor relationship in the YRD can be accomplished through the identification of the

63   geophysical sources as well as sectoral sources contribution. Such information is considerable for

64   designing adequate control strategies regarding tropospheric O_3 concentration. Furthermore,

65   process analysis tool provides an insight on qualitative and quantitative contributions of

66   individual atmospheric processes.

67
68   **METHODOLOGY AND DATA**
69

70　*Model description and setup*

71　　We apply an air quality model CAMx v6.20 (ENVIRON, 2015) to simulate an O_3 episode

72　from 25 July to 6 August, 2015. CAMx simulates the emission, advection, dispersion, chemical

73　transformation and physical removal of air pollutants on an Eulerian three-dimensional grid. Fig.

74　1 shows the model domain used in this study, which has a 265×265 grids at 9 km resolution on a

75　Lambert conformal map projection. Vertically, we use 20 terrain-following layers from the

76　surface to 20 km, with the lowest 10 layers below 2 km. The meteorological conditions were

77　provided from the Weather Research and Forecasting model (WRF v3.2.1,

78　http://www2.mmm.ucar.edu/wrf/users/docs/user_guide_V3.2/ARWUsersGuideV3.pdf), using

79　NCEP/NCAR FNL reanalysis data (1°×1°) for initial and boundary conditions. Four-dimensional

80　data assimilation (Otte, 2009), based on 6-h 3-D analyses of temperature, water vapor mixing

81　ratio and horizontal wind speeds, was used with a nudging coefficient of 3.0×10^{-4} for all the

82　above components over this domain. Monthly-average concentrations from the MOZART model

83　were used for chemical boundary conditions. The simulation was made from 14 July to 7 August

84　2015, using the first four days as a spin-up period.

85　　The anthropogenic emissions in China were obtained from the Multi-resolution Emission

86　Inventory for China (MEIC, http://www.meicmodel.org/) at 0.25°×0.25° resolution, while

87　emissions in other countries were derived from the bottom-up Regional Emission inventory in

88　Asia (REAS 2.1) (Kurokawa et al., 2013). To improve the distribution of anthropogenic

89   emissions at the 9 km resolution used here, we spatially reallocated the coarse resolution

90   emissions over East Asia based on relevant proxies. For example, residential emissions were

91   spatially allocated by population data; vehicle emissions were distributed according to road

92   length data; and agricultural emissions were allocated based on cropland intensity data. All the

93   static data including population, road length and land category data are obtained through

94   http://www.dsac.cn, with spatial resolution of 1km and data year of 2015. Biogenic emissions

95   were obtained from a biogenic emission model (MEGANv2) provided by NCAR

96   (http://accent.aero.jussieu.fr/database_table_inventories.php).

97   In this study, we use surface NO_2 and O_3 concentration measurements from a monitoring

98   network maintained by the Ministry of Environmental Protection (http://106.37.208.233:20035).

99   The locations of surface sites (273 sites within the model domain) are shown in Fig. 1. Hourly

100   meteorological variables (wind, temperature, relative humidity and solar radiation) were taken

101   from automatic meteorological stations operated by the Shanghai Meteorological Service, and the

102   data shown in Fig. 2 was collected at Pudong station (31.22°N, 121.55°E), which represents an

103   urban area in Shanghai.

104

105   ***Source apportionment***

106   O_3 source apportionment technology (OSAT, Yarwood et al., 1996) uses multiple tracer

107   species to track the fate of O_3 and its precursors by monitoring the effects of emissions, chemical

108   reactions, transport, diffusion and deposition within CAMx. These tracers allow O_3 formation

109   from multiple "source groupings" to be tracked simultaneously within a single simulation. A

110   source grouping is defined in terms of geographical area and/or emission category, and the

111   CAMx boundary conditions (BC) and initial conditions (IC) are tracked as separate source

112   groupings. OSAT employs four types of tracers for each source grouping: N_i and V_i (tracking

113   NO_x and VOCs originating from source grouping i, respectively), and O_3N_i and O_3V_i (tracking O_3

114   formation under NO_x-limited and VOCs-limited conditions attributed to source grouping i,

115   respectively). The ratio of the production rates of hydrogen peroxide to nitric acid is used as an

116   indicator of the O_3 formation sensitivity to VOCs and NO_x. Sillman (1995) proposed that O_3

117   formation is NO_x-limited when the ratio exceeds 0.35 and VOCs-limited when the ratio is less

118   than 0.35. The O_3N and O_3V tracers for each source grouping accumulate a weighted fraction of

119   the O_3 production (ΔO_3) that occurs in each grid cell at each time step (Δt):

120

$$O_3N_i(t + \Delta t) = O_3N_i(t) + \Delta O_3 \times N_i(t) / \sum_{i=1}^{m} N_i(t)$$

$$O_3V_i(t + \Delta t) = O_3V_i(t) + \Delta O_3 \times V_i(t) \times \kappa OH_i / \sum_{i=1}^{m} [V_i(t) \times \kappa OH_i]$$

121

122   Where t represents time, m is the number of source groupings, and κOH_i is the average OH rate

123   constant of VOCs for the i source grouping (ENVIRON, 2015).

124

Source regions and source categories

Targeting a spatial-source analysis, we divide the model domain into eight source receptor

areas based on province boundaries: Shanghai (SH), provinces north of Shanghai (NORTH2SH),

provinces south of Shanghai (SOUTH2SH), northern China (NORTH_CHN), western China

(WEST_CHN), southern China (SOUTH_CHN) and regions outside China (OUT_CHN) (see

Fig. 1). NORTH2SH consists of Jiangsu, Anhui and Shandong provinces and SOUTH2SH

consists of Zhejiang, Jiangxi and Fujian provinces.

Anthropogenic emissions from MEIC are categorized into industry, transport, residential,

energy and agricultural sectors. Biogenic emissions are generated from the MEGAN model.

These six categories, are defined as source groupings in the OSAT model. In addition, the initial

and boundary conditions (IC and BC) are treated as individual source groupings.

Process analysis

Process analysis (PA) allows for in-depth analysis of the contributions from individual physical

and chemical processes operating within the model (Jeffries and Tonnesen, 1994). Using this

approach, it is possible to investigate the complex interactions between different processes, and

explain simulation results within the context of the model formulation. Integrated process rate

analysis provides detailed rate information for each process in CAMx (i.e., advection, diffusion,

143   deposition, emissions and chemistry) for selected grid cells and selected species (Wang et al.,

144   1995).

145

146   *Sensitivity analysis*

147   Sensitivity analysis is a widely used approach in which sources are quantified by perturbing

148   emissions one at a time and simulating the difference in pollutant concentrations compared to

149   unperturbed control scenarios. There are four sensitivity simulations as well as control run

150   (BASE). Each sensitivity simulation is compared to the BASE run in order to assess the response

151   of O_3 to emission perturbations during the episode.

152

153   **RESULTS AND DISCUSSIONS**

154

155   *The episode review and model evaluation*

156   The daily maximum temperature is more than 35℃ for sustained 10 days from 27 July to 5

157   August 2015, in which 4 days of maximum temperature are over 37℃, which is a very powerful

158   heat wave in Shanghai (Fig. 2). In the meantime, a continuous (12 days) O_3 pollution episode was

159   detected in Shanghai over the Yangtze River Delta (YRD) region, in which the daily maximum

160   8-h moving average O_3 concentrations in 4 days exceeded moderately polluted level (>100 ppbv),

161   with the other 8 days exceeding lightly polluted level (>75 ppbv). The hourly maximum observed

162   O_3 concentration reached up to 130 ppbv, which significantly exceeded the moderately polluted

163   level. During this period, the western Pacific subtropical high stayed over YRD region, and

164   thereby leaded to this powerful heat wave in Shanghai. The relative humidity ranged from 40% to

165   80% and the total radiation, a key meteorological factor for O_3 formation, reached 1000 W/m^2,

166   indicating that skies were clear. There is typically a positive correlation between O_3 and

167   temperature because of a combination of meteorological and chemical factors. High temperatures

168   lead to higher emissions of some O_3 precursors, greater electrical energy use, and more biogenic

169   VOC emissions.

170   Fig. 2 also compares the simulated meteorological and O_3 concentration with observations, to

171   assess the performance of the model. Before 27 July, there were lower temperatures, higher

172   relative humilies, lower total radiation and lower O_3 concentrations. The comparisons

173   demonstrate that the model can capture the temporal variation of meteorological variables over

174   the study period very well compared to observations. To evaluate how well the model captures

175   the diurnal cycle of O_3, we calculate the episode-mean hourly O_3 concentrations, see Fig. 3. We

176   find that the model catches the high O_3 during daytime but underestimates O_3 at nighttime. This

177   may be due to overestimated NO emissions that leads to much chemical destruction at nighttime

178   (Awang et al., 2015).

179   Fig. 4 shows the weather charts (http://web.kma.go.kr/chn/weather/images/analysischart.jsp) at

180   00UTC (08LST) each day. A subtropical high pressure is noted near Taiwan on 30 July, and the

181   center moves north on 1 August. This synoptic pattern is disturbed when a typhoon approaches

182   from the Pacific Ocean. The left panels display the simulated wind fields at the corresponding

183   times (08:00LST), and daytime average O_3 concentrations (from 08:00 to 18:00 LST). The wind

184   fields show that there was a high pressure over the ocean and the location is consistent with that

185   in the weather charts on 30 July and 1 August. A southwesterly wind was induced by the high

186   pressure prevailing along the east coast of China during the polluted heat wave period. The

187   spatial distribution of O_3 shows that there were high concentrations in the north of China as well

188   as on the east coast. On 6 August, the approaching typhoon brought easterly winds to Shanghai

189   and the Yangtze River Delta region, along with cleaner marine air.

190   A suite of statistical metrics are considered to judge the performance of the model. We use the

191   correlation coefficient (R), mean value of the observation (Obs) and simulation (Mod), root mean

192   square error (RMSE) and mean bias (MB) of the hourly data over the full 20-day period. The

193   spatial distributions of R and RMSE for each city are displayed in Fig. 5. The simulation

194   generally agrees well with the observations and the correlation coefficients are greater than 0.7

195   for most of the cities. The RMSEs are below 15 ppbv in south China, but are 15-30 ppbv in north

196   China. Table 1 summarizes the statistical metrics for O_3 and NO_2 for each region separately

197 (region definitions are shown in Fig. 1). The correlation coefficients (R) for O_3 are typically

198 0.6-0.8, indicating that the model can reproduce the O_3 variations well in the study period. The R

199 values for NO_2 are lower than for O_3, with values of 0.5-0.7. The mean bias shows that simulated

200 O_3 concentrations were underestimated over Shanghai (SH) and SOUTH2SH regions, but

201 overestimated for the other regions. NORTH_CHN was the only region where NO_2 was

202 underestimated. In comparing different regions, it is worth noting that the model performed best

203 over Shanghai and least well over NORTH_CHN. The NO_x emission over NORTH_CHN may be

204 underestimated, and this is consistent with overestimation of O_3 due to less urban titration. In

205 general, based on this analysis, we infer that the CAMx model performs relatively well in

206 simulating observed O_3 concentrations.

207   Fig. 6 shows a scatterplot of hourly daytime O_3 from the model and the observations at some

208 points. The selected cities are Shanghai, Nanjing, Hangzhou, Hefei, Fuzhou, Nanchang, Jinan,

209 Beijing, Changsha, Wuhan, Guangzhou and Xi'an, which are capitals of each province,

210 respectively, over the east China (displayed in red points in Fig. 1). These data help to assess the

211 model performance, showing that there is clearly a correlation between the model and

212 observations, with he averaged correlation coefficient (R) of 0.69. The standard linear least

213 square regression analysis reveals that the model somewhat overestimates the daytime O_3

214 concentrations.

215

216   *Source contribution analysis*

217   Fig. 7 shows the daytime-average (08:00 – 18:00 LST) contributions to O_3 for Shanghai area

218   from different source regions and source categories. We find that Shanghai and SOUTH2SH are

219   the two regions that contributed the most to O_3 concentrations in Shanghai, together reaching as

220   much as 90%. This is a consequence of the southwesterly flow during the study period (see Fig. 2

221   and 4), which brought pollutants and precursor emissions to Shanghai. In this period, the

222   contributions from other regions were insignificant. The contributions of different emission

223   categories show that the industrial sector contributes the most, followed by energy, biogenic and

224   transport sectors. As expected, initial conditions (IC) were the major contributor at the beginning

225   of the simulation, and it decreased significantly over the period. The contribution of boundary

226   conditions (BC) was remarkably large on August 6, and this reflects the dominance of easterly

227   flow in the Shanghai area on this day (see Fig. 4(c)).

228   Since Shanghai and SOUTH2SH are the dominant sources of O_3 in Shanghai during this

229   episode, it is interesting to examine the source apportionment by emission category from these

230   two regions. For local emissions in Shanghai area (Fig. 8(a)), Industrial emissions were the

231   largest source, with a contribution of 43%, and the contributions from energy, transport and

232   biogenic sectors were 20%, 20% and 10%, respectively. In contrast (Fig. 8(b)), the largest source

233   from SOUTH2SH region was not from industrial emissions but from energy and biogenic

234   emissions which provided 28% and 28% of the O_3 from this region to Shanghai. The

235   contributions from industry and transport tailed off to 25% and 11%, respectively. In addition,

236   5-6% of O_3 in Shanghai was attributed to initial and boundary conditions (IC+BC), and

237   agriculture and residential emissions contributed very little.

238   The average diurnal O_3 contributions for Shanghai area from different source regions during

239   the episode period are shown in Fig. 9(a). It is clear that local and non-local emissions show

240   distinct characteristics. The contribution of local emissions in Shanghai is heavily peaked,

241   increasing during the morning, and with a maximum value around noontime. This is strongly

242   related to chemical formation of O_3 when solar radiation is high. The contributions from

243   non-local sources (mostly from SOUTH2SH) are greatest in the morning and afternoon. During

244   nighttime O_3 is destroyed through titration by reaction with NO, and there is no O_3 formation

245   without solar radiation. Consequently, most of the O_3 in Shanghai originates by transport from

246   surrounding areas, and the contributions during nighttime are from non-local sources. The

247   contribution of different source categories is shown in Fig. 9(b). The contribution of industrial

248   emissions reveals similar features to the local emission in Shanghai, increasing during the

249   morning, and reaching a maximum at noon. The contributions from energy, transport and

250   biogenic emissions remain relatively similar over the course of daytime.

251   To evaluate the source contributions in this study, and to inform mitigation strategies for O_3 in

252   Shanghai, several sensitivity simulations are conducted individually (described in Table 2). The

253   sensitivity simulation results show that if all anthropogenic emissions in Shanghai were reduced

254   by 50% (SH0.5), the O_3 levels in Shanghai would have decreased by 12% compared to the base

255   run (BASE). When industrial or transport emissions were reduced by 50% in both Shanghai and

256   SOUTH2SH (IND0.5 and TRA0.5), the decrease in O_3 concentrations was 11% or 6%,

257   respectively. If all industrial and transport emissions in both regions were reduced by 50%, the O_3

258   concentrations would decrease by 18%. This sensitivity analysis clearly demonstrates that the

259   response of O_3 to emission reductions isn't linear. And this leads to discrepancy between

260   sensitivity analysis and source apportionment results. Because O_3 are most formed by chemical

261   formations, the sensitivity simulations do not generate or lose equivalent concentrations of

262   secondary O_3 when the simulations are run with fewer precursors. The Source apportionment

263   method, which does not change any physical and chemical processes, can objectively allocate

264   100% of the target O_3 to specified sources. Besides, the reduction of O3 in IND_TRA0.5 run is

265   the biggest, even more significant than those in SH0.5 run. This illustrates that industrial and

266   transport emissions are the main source of precursors in generating O_3 in Shanghai, and should be

267   considered as the major target sectors for emission controls.

268

269   ***Process analysis***

270   The contributions of each modeled process to changes in O_3 in the model are calculated as

271   average hourly values for each grid cell. Average rates in the surface layer for Shanghai area

272 from July 27 0000 LST to August 5 2300 LST are shown in Fig. 10. The atmospheric processes

273 that influence O_3 concentrations include chemistry, horizontal and vertical advection, horizontal

274 and vertical diffusion and dry deposition. Positive values indicate that O_3 concentrations are

275 increased by the process and negative values indicate a decrease. Note that there is no primary

276 emission of O_3, so this process makes no direct contribution to O_3.

277   The diurnal cycle of O_3 concentration reveals that the build-up of O_3 in the morning is typically

278 more rapid than the decline in the evening. During daytime, the model has a tendency to generate

279 a broad daytime O_3 maximum, with the highest concentrations reached at noon. In the morning,

280 chemical production dominates as the solar radiation increases, and there is little removal by

281 deposition while O_3 remains low. Consequently, O_3 concentrations start to rise rapidly in the

282 morning. The effect of chemical processes remains positive from 0600LST to 1600LST, while at

283 other times there is net chemical destruction of O_3 by titration. Horizontal advection of O_3 from

284 neighboring regions also keeps daytime concentrations high. In contrast, vertical advection

285 contributes to a decrease of O_3 as vertical mixing is enhanced during daytime, carrying O_3 away

286 from the surface. The results also reveal that vertical diffusion has an important role in increasing

287 O_3 concentrations during afternoon and nighttime. We note above that the model underestimates

288 the low O_3 levels at nighttime. This may be due to too much chemical destruction, excessive dry

289 deposition, or to horizontal advection (see Fig. 9). While this may be a consequence of

290 overestimated NO emissions or errors in dry deposition parameters, it may also reflect

291 meteorological factors such as insufficient boundary layer mixing at nighttime. To summarize,

292 chemical production, horizontal advection and vertical diffusion are the main contributors to

293 increases in O_3 concentrations during daytime, while deposition and vertical advection reduce O_3

294 concentrations.

295

296 **CONCLUSIONS**
297

298   A sustained, 10-day episode of high O_3 occurred in the Yangzte River Delta from 27 July to 5

299 August 2015, with O_3 concentrations in the afternoon reaching more than 100 ppbv. During this

300 O_3 episode, temperatures of more than 35°C and sunny stagnant meteorological conditions were

301 observed, providing favorable conditions for O_3 formation. A numerical model was used to study

302 this O_3 episode and comparisons between simulation and observations suggest that the model can

303 reproduce the meteorological and chemical conditions during this O_3 episode well.

304   By applying source apportionment approaches, we have developed a detailed understanding of

305 the precursor source region and source category contributions to surface O_3 in Shanghai.

306 Spatially, precursors from local and nearby southerly provinces contributed 90% of O_3

307 concentrations in this episode. Normally synoptic high pressure systems in summertime over this

308 region are associated with high temperatures and a southwesterly wind which brings O_3 and its

309 precursors to Shanghai. Industrial emission was the largest local source, with a contribution of

310   41%, and the contributions from energy, transport and biogenic sectors were 19%, 19% and 12%,

311   respectively. For precursors from southern provinces, energy and biogenic sectors were the

312   largest sources, with contributions of 30% and 29%. Therefore, it is a priority to reduce

313   industrial, energy and transport emissions through effective O_3 control strategies. However,

314   biogenic emissions also play an important role in formation of O_3 at this time of year.

315   We have analyzed the contributions from individual physical and chemical processes during

316   this episode. It is interesting to note that the build-up of O_3 in the morning was much more rapid

317   than the decline in the evening. In the morning, chemical production made a large contribution in

318   the presence of sunlight, while the removal of O_3 was much smaller. The results revealed that

319   chemical production, horizontal advection and vertical diffusion contribute to the increase of O_3

320   concentrations during daytime. The underestimation of O_3 at nighttime may be due to too much

321   destruction by chemistry, deposition or horizontal advection. This may be a consequence of

322   overestimated NO emissions or errors in dry deposition parameters, it may also reflect

323   meteorological factors such as insufficient boundary layer mixing at nighttime.

324

331 **REFERENCES**

332

333 Awang, N.R., Ramli, N.A., Yahaya, A.S. and Elbayoumi, M. (2015). High nighttime

334 ground-level ozone concentrations in Kemaman: NO and NO2 concentrations attributions.

335 *Aerosol Air Qual. Res.* 15(4): 1357-1366.

336 Cohan, D.S., Boylan, J.W., Marmur, A. and Khan, M.N. (2007). An integrated framework for

337 multipollutant air quality management and its application in Georgia. *Environ. Manage.* 40:

338 545-554.

339 Crutzen, P.J., Lawrence, M.G. and Ulrich, P. (1999). On the background photochemistry of

340 tropospheric ozone. *Tellus B,* 51: 123-146.

341 Ding, A. J., Fu, C. B., Yang, X. Q., Sun, J. N., Zheng, L. F., Xie, Y. N., Herrmann, E., Nie, W.,

342 Petäjä, T., Kerminen, V.-M., and Kulmala, M. (2013). Ozone and fine particle in the western

343 Yangtze River Delta: an overview of 1-yr data at the SORPES station, *Atmos. Chem. Phys.*, 13,

344 5813–5830.

345 Ding, A.J., Wang, T., Thouret, V., Cammas, J.P. and Nédélec, P. (2008). Tropospheric ozone

346 climatology over Beijing: Analysis of aircraft data from the MOZAIC program. *Atmos. Chem.*

347 *Phys.* 8: 1-13.

348 ENVIRON (2015). The Comprehensive Air quality Model with extensions (CAMx), version

349 6.20. (Available from http://www.camx.com).

350 Fann, N. and Risley, D. (2013). The public health context for PM2:5 and ozone air quality trends,

351   *Air Qual. Atmos. Hlth.*, 6, 1–11.

352   Feng, Z. W., Jin, M. H., Zhang, F. Z., and Huang, Y. Z. (2003). Effects of ground-level ozone

353   (O-3) pollution on the yields of rice and winter wheat in the Yangtze River Delta, *J. Environ.*

354   *Sci.-China*, 15, 360–362.

355   Geng, F. H., Tie, X. X., Xu, J. M., Zhou, G. Q., Peng, L., Gao, W., Tang, X., and Zhao, C. S.

356   (2008). Characterizations of ozone, NOx , and VOCs measured in Shanghai, China, *Atmos.*

357   *Environ.*, 42, 6873–6883.

358   Huang, J. P., Fung, J. C. H., and Lau, A. K. H. (2006). Integrated processes analysis and

359   systematic meteorological classification of ozone episodes in Hong Kong, *J. Geophys.*

360   *Res.-Atmos.*, 111, D20309.

361   Jeffries, H.E. and Tonnesen, S. (1994). A comparison of two photochemical reaction mechanisms

362   using mass balance and process analysis. *Atmos. Environ.* 28: 2991-3003.

363   Jiang, F., Zhou, P., Liu, Q., Wang, T. J., Zhuang, B. L., and Wang, X. Y. (2012). Modeling

364   tropospheric ozone formation over East China in springtime, *J. Atmos. Chem.*, 69, 303–319.

365   Kumar, U., Prakash, A. and Jain, V.K. (2008). A photochemical modeling approach to investigate

366   o3 sensitivity to NOx and VOCs in the urban atmosphere of Delhi. *Aerosol Air Qual. Res.* 8:

367   147-159.

368   Kurokawa, J., Ohara, T., Morikawa, T. and Hanayama, S. (2013). Emissions of air pollutants and

369   greenhouse gases over asian regions during 2000–2008: Regional emission inventory in Asia

370   (reas) version 2. *Atmos. Chem. Phys.* 13: 11019-11058.

371   Landry, J. S., Neilson, E. T., Kurz, W. A., and Percy, K. E. (2013). The impact of tropospheric

372   ozone on landscape-level merchantable biomass and ecosystem carbon in Canadian forests,

373   *Eur. J. Forest Res.*, 132, 71–81.

374   Otte, T.L. (2009). The impact of nudging in the meteorological model for retrospective air quality

375   simulations. Part I: Evaluation against national observation networks. *J. App. Meteor. &*

376   *Climatology* 47: 1853-1867.

377   Ran, L., Zhao, C.S., Geng, F., Tie, X., Tang, X., Peng, L., Zhou, G., Yu, Q., Xu, J., Guenther, A.

378   (2009). Ozone photochemical production in urban Shanghai, China: Analysis based on ground

379   level observations. *J. Geophys. Res.* 114: 4228-4240

380   Shao, M., Tang, X., Zhang, Y. and Li, W. (2006). City clusters in china: Air and surface water

381   pollution. *Front. Ecol. Environ.* 4: 353-361.

382   Shao, M., Zhang, Y., Zeng, L., Tang, X., Zhang, J., Zhong, L. and Wang, B. (2009).

383   Ground-level ozone in the pearl river delta and the roles of VOC and NOx in its production. *J.*

384   *Environ. Manage.* 90: 512-518.

385   Shu, L., Xie, M., Wang, T., Gao, D., Chen, P., Han, Y., Shu, L, Zhuang, B. and Li, M. (2016).

386   Integrated studies of a regional ozone pollution synthetically affected by subtropical high and

387   typhoon system in the Yangtze River Delta region, China. *Atmos. Chem. Phys.* 16:

388   15801-15819.

389   Sillman, S. (1995). The use of no y , h2o2, and hno3 as indicators for ozone-no x -hydrocarbon

390   sensitivity in urban locations. *J. Geophys. Res.* 100: 14175-14188.

391   Streets, D.G., Fu, J.S., Jang, C.J., Hao, J., He, K., Tang, X., Zhang, Y., Wang, Z., Li, Z. and

392   Zhang, Q. (2007). Air quality during the 2008 Beijing Olympic Games. *Atmos. Environ.* 41:

393   480-492.

394   Tang, G., Li, X., Wang, Y. and Xin, J. (2009). Surface ozone trend details and interpretations in

395   Beijing, 2001–2006. *Atmos. Chem. Phys.* 9: 8813-8823.

396   Wang, H. X., Zhou, L. J., and Tang, X. Y. (2006b). Ozone concentrations in rural regions of the

397   Yangtze Delta in China, *J. Atmos. Chem.*, 54, 255–265.

398   Wang, T., Cheung, V.T.F., Anson, M. and Li, Y.S. (2001). Ozone and related gaseous pollutants

399   in the boundary layer of eastern china: Overview of the recent measurements at a rural site.

400   *Geophys. Res. Lett.* 28: 2373-2376.

401   Wang, T., Wei, X.L., Ding, A.J. and Poon, C.N. (2009). Increasing surface ozone concentrations

402   in the background atmosphere of southern china, 1994–2007. *Atmos. Chem. Phys.* 9:

403   6217-6227.

404   Wang, Z., Langstaff, J.E. and Jeffries, H.E. (1995). The Application of the Integrated Process Rate

405   Analysis Method for Investigation of Urban Airshed Model (UAM) Sensitivity to Speciation in

406   VOC Emissions Data. Air & Waste Management Association annual meeting, San Antonio, TX.

407   Wang, Z., Li, J., Wang, X., Pochanart, P. and Akimoto, H. (2006a). Modeling of regional high

408   ozone episode observed at two mountain sites (mt. Tai and Huang) in east china. *J. Atmos.*

409   *Chem.* 55: 253-272.

410   Wild, O., Prather, M.J., Akimoto, H., Sundet, J.K., Isaksen, I.S.A., Crawford, J.H., Davis, D.D.,

411   Avery, M.A., Kondo, Y., Sachse, G.W. and Sandholm, S.T. (2004). Chemical transport model

412   ozone simulations for spring 2001 over the western pacific: Regional ozone production and its

413   global impacts. *J. Geophys. Res.* 109:-.

414   Xie, M., Zhu, K. G., Wang, T. J., Chen, P. L., Han, Y., Li, S., Zhuang, B. L., and Shu, L. (2016).

415   Temporal characterization and regional contribution to O3 and NOx at an urban and a

416   suburban site in Nanjing, China, *Sci. Total Environ.*, 551, 533–545.

417   Xu, X., Lin, W., Wang, T., Yan, P., Tang, J., Meng, Z., and Wang, Y. (2008). Long-term trend of

418   surface ozone at a regional background station in eastern China 1991–2006: enhanced

419   variability, *Atmos. Chem. Phys.* 8, 2595-2607

420   Yang, H.H., Chen, H.W., Chi, T.W. and Chuang, P.Y. (2008). Analysis of atmospheric ozone

421   concentration trends as measured by eighth highest values. *Aerosol Air Qual. Res.* 8: 308-318.

422   Yarwood, G., Morris, R.E., Yocke, M., Hogo, H. and Chico, T. (1996). Development of a

423   Methodology for Source Apportionment of Ozone Concentration Estimates from a

424   Photochemical Grid Model. Presented at the 89th AWMA Annual Meeting, Nashville TN,

425   June 23-28.

426   Zhang, Y.H., Hu, M., Zhong, L.J., Wiedensohler, A., Liu, S.C., Andreae, M.O., Wang, W. and

427   Fan, S.J. (2008). Regional integrated experiments on air quality over pearl river delta 2004

428   (pride-prd2004): Overview. *Atmos. Environ.* 42: 6157-6173.

429

430

431

432 **Table 1.** Statistical summary of the model results against observations between 00:00LST 18
433 July and 00:00LST 7 August.

Species	Regions	N[a]	Obs[b]	Mod[c]	R[d]	RMSE[e]	MB[f]
O₃ (ppbv)	Shanghai(SH)	478	46.5	40.0	0.80	14.7	-6.5
	NORTH2SH	32962	32.8	41.4	0.71	21.6	8.6
	SOUTH2SH	16108	26.9	23.9	0.76	13.6	-3.0
	NORTH_CHN	23400	36.5	46.9	0.61	28.7	10.4
	WEST_CHN	40000	32.1	38.7	0.78	21.2	8.5
	SOUTH_CHN	15768	21.1	25.9	0.68	15.7	4.8
NO₂ (ppbv)	Shanghai(SH)	478	15.4	17.8	0.69	10.7	2.4
	NORTH2SH	32961	11.7	14.6	0.52	11.1	2.9
	SOUTH2SH	16110	9.1	12.8	0.63	12.9	3.8
	NORTH_CHN	23405	11.0	8.8	0.50	8.6	-2.2
	WEST_CHN	40093	10.2	12.5	0.52	13.0	2.2
	SOUTH_CHN	15771	7.9	10.7	0.58	10.4	2.8

434 [a] Number of valid paired data.

435 [b] Mean value of observations

436 [c] Mean value of simulations

437 [d] Correlation coefficient

438 [e] Root mean square error

439 [f] Mean bias

440

441   **Table 2.** Sensitivity analysis of emission perturbations in specific regions.

Simulation	Description	Average O$_3$ (ppbv) In Shanghai [a]	Contribution of sensitivity (%) [b]
BASE	With base emission	91.3	/
SH0.5	50% reduced anthropogenic emission in Shanghai (SH)	80.4	-12
IND0.5	50% reduced industry emission in Shanghai (SH) and SOUTH2SH	82.3	-11
TRA0.5	50% reduced transport emission in Shanghai (SH) and SOUTH2SH	86.3	-6
IND_TRA0.5	50% reduced industry and transport emission in Shanghai (SH) and SOUTH2SH	77.4	-18

442   [a] The O$_3$ concentration is averaged during daytime (08:00-18:00 LST) from July 27 to August 5
443   2015.

444   [b] Contribution $= \frac{Sensitivity - BASE}{BASE} \times 100\%$

445
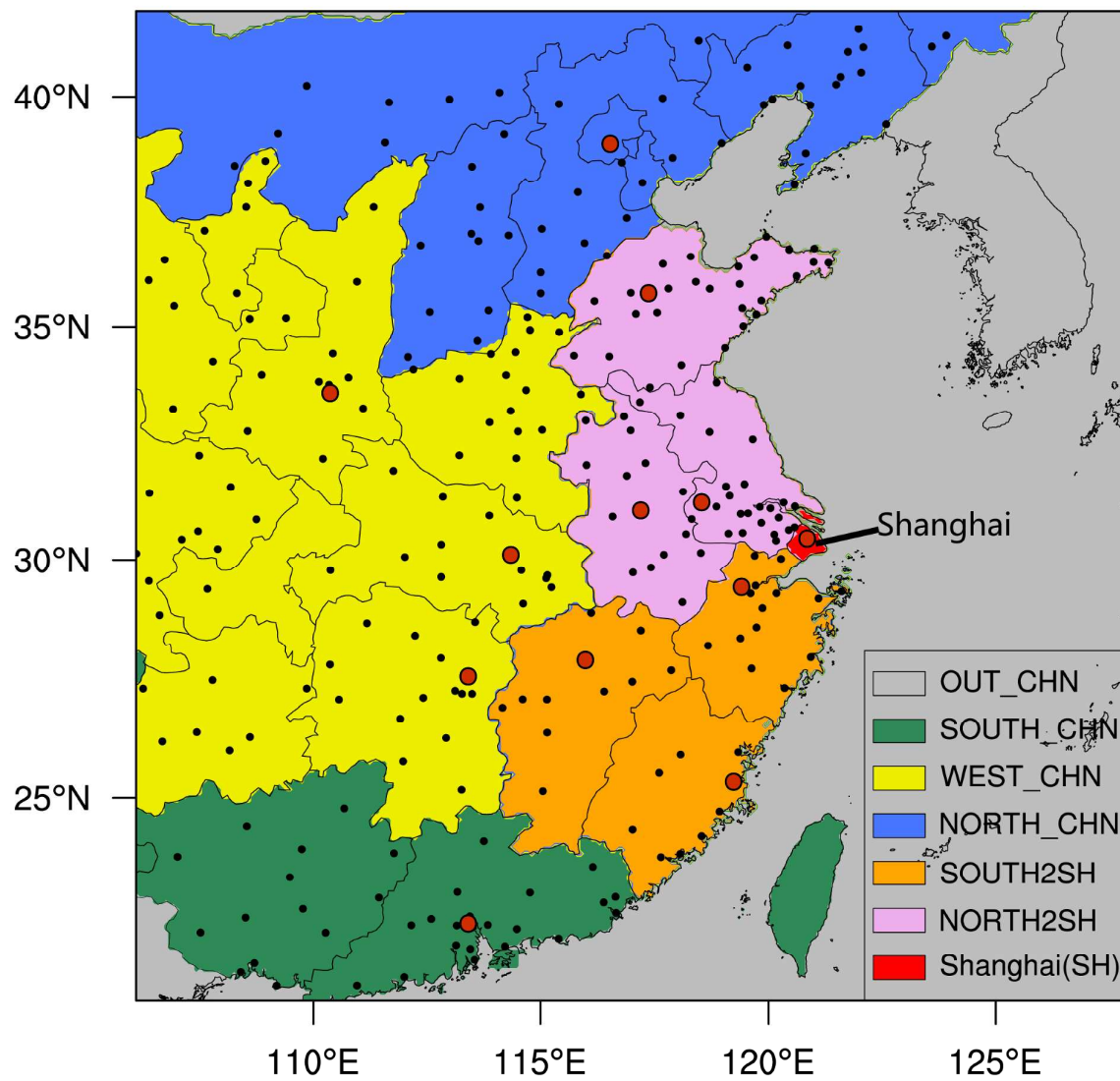
446

447 **Fig. 1.** Model domain showing the sub-division into separate areas for geographic source

448 apportionment (shaded) and surface observation sites (black dot), and the red dots are the selected

449 cities for scatterplot.

450

451
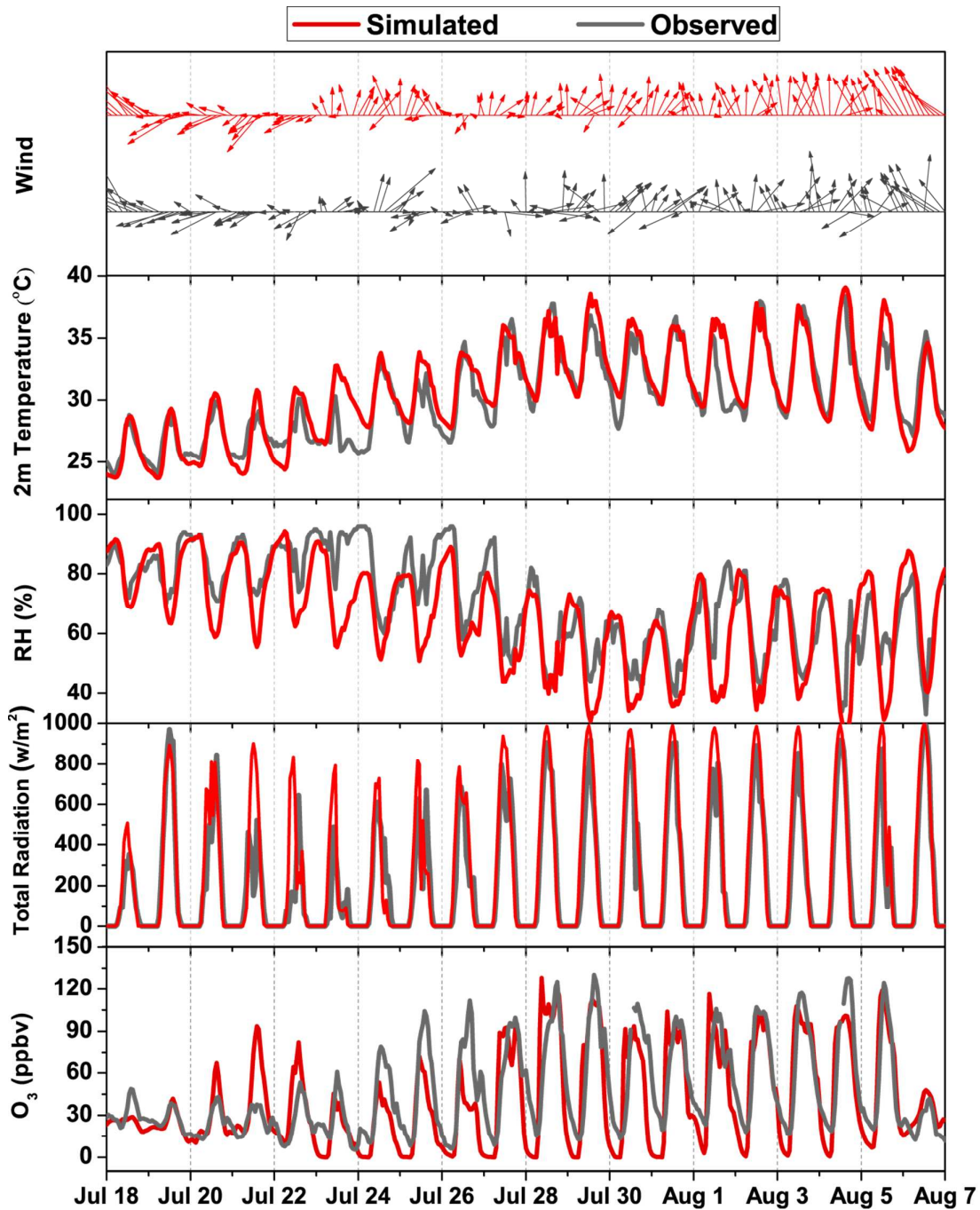
Fig. 2. Comparison of hourly time-series for simulated (red) and observed (gray) wind, 2-m

temperature, relative humidity, total radiation and ozone concentration at Shanghai station from

18 July to 7 August 2015.

455

456

457

458
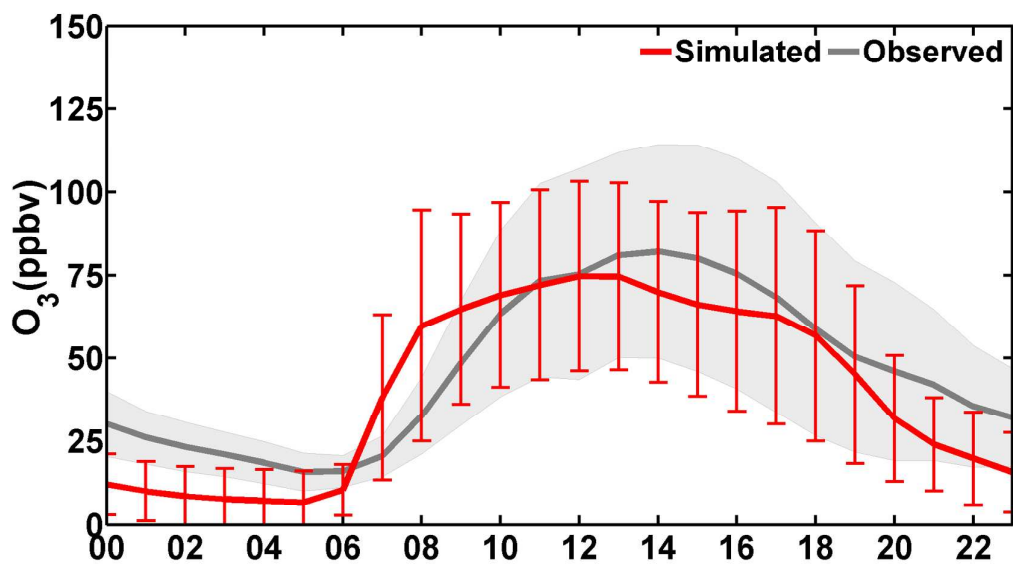
Fig. 3. Comparison of the diurnal cycle of simulated and observed O_3 at Shanghai station from July 27 to August 5, 2015. Error bars (lines for simulation, shaded for observation) show the standard deviation for each hour.

463

464

465

466

(a) 08:00LST, 30 July
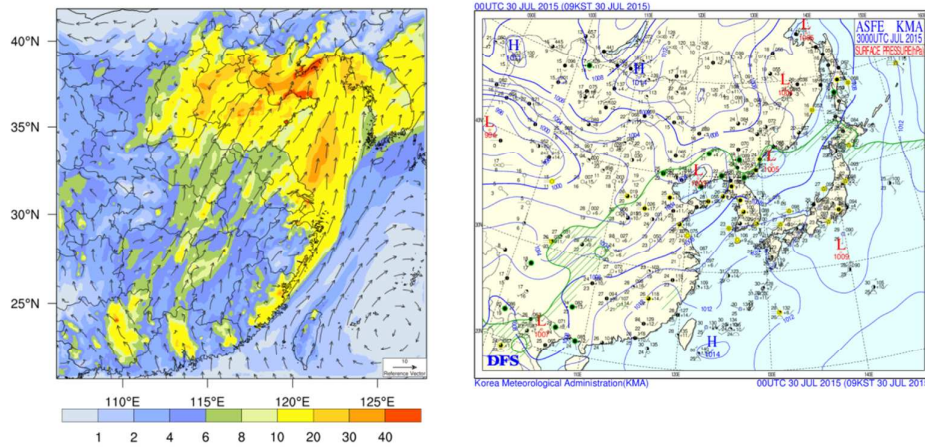
(b) 08:00LST, 1 August
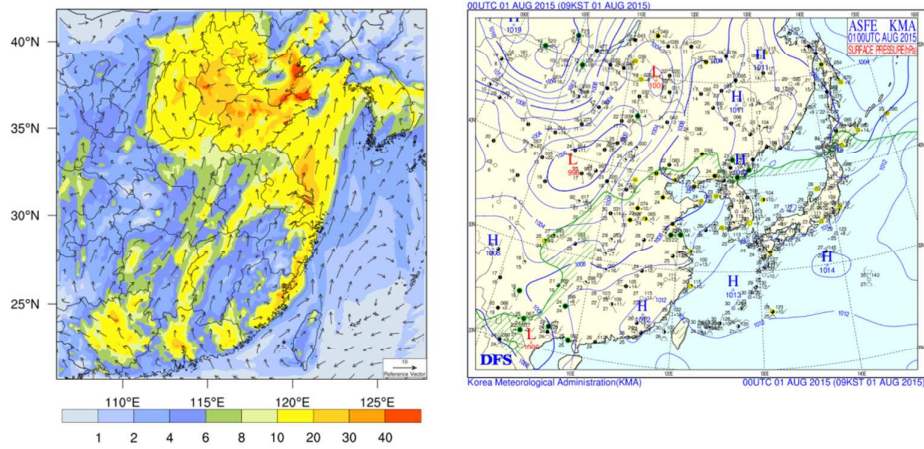
(c) 08:00LST, 6 August

467
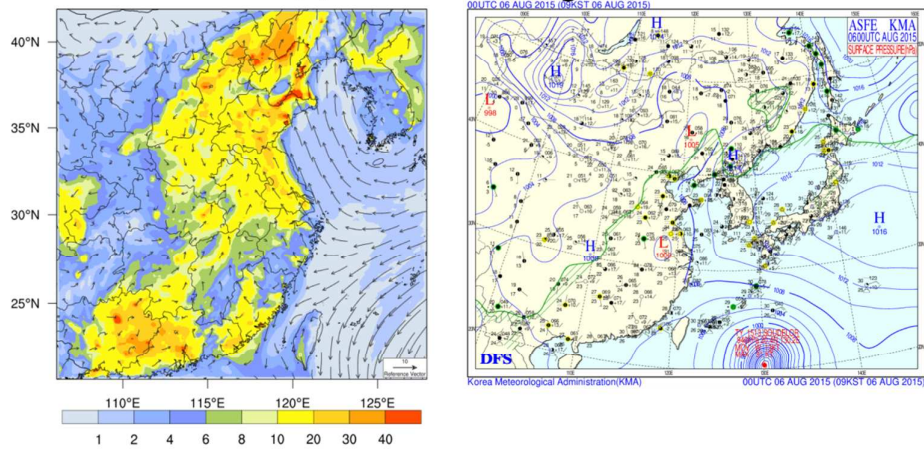
468   **Fig. 4.** Simulated wind (left) and surface synoptic charts
469   (right, http://web.kma.go.kr/chn/weather/images/analysischart.jsp) at 08:00 LST on 30 July, 1
470   August and 6 August 2015. Daytime averaged (08:00-18:00 LST) simulated ozone
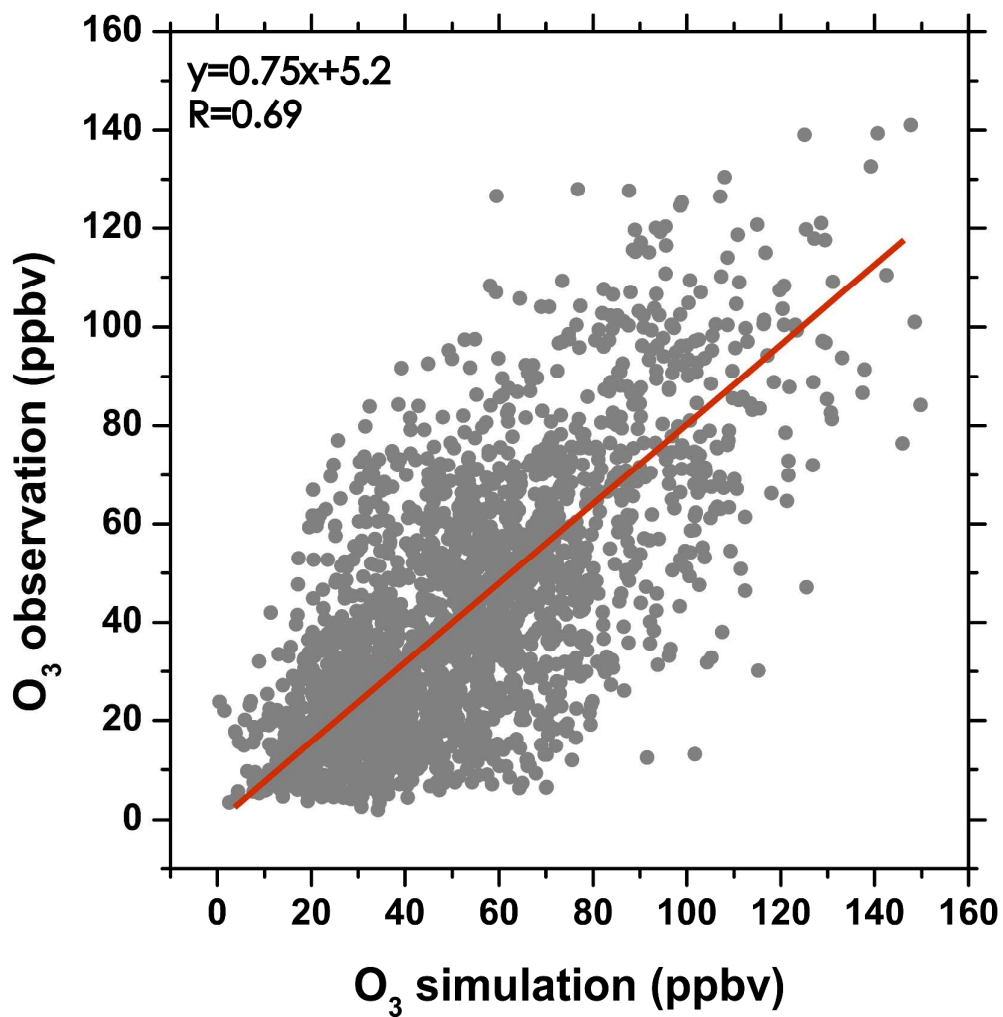471   concentration (shaded) are also plotted on the left.

472

473

474

475
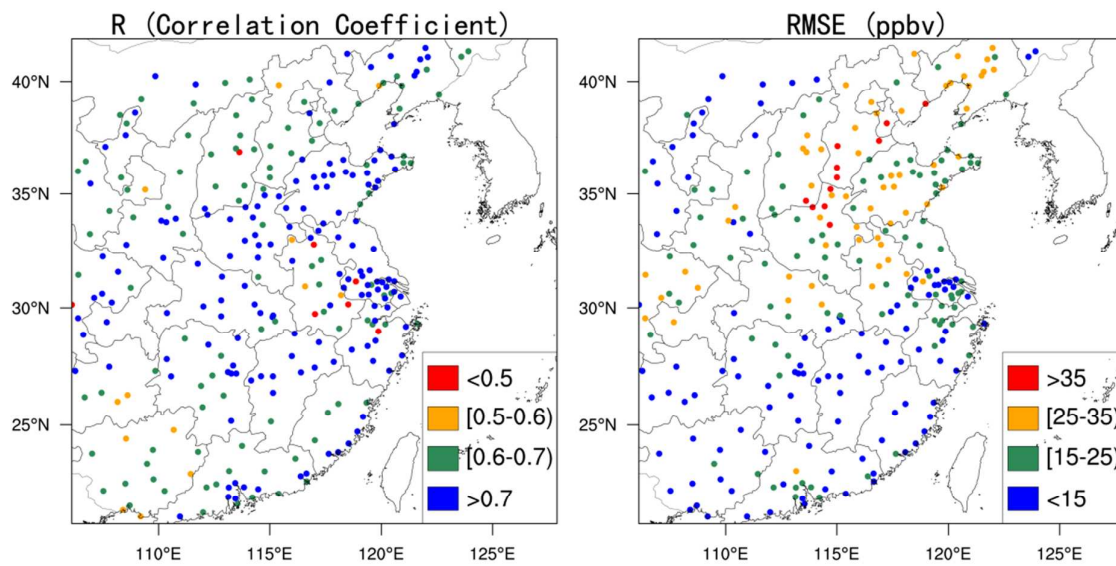
Fig. 5. Spatial patterns of correlation coefficients (R) and root mean square errors (RMSE) for

ozone between 00:00LST 18 July and 00:00LST 7 August.

478

y=0.75x+5.2
R=0.69

O₃ observation (ppbv)

O₃ simulation (ppbv)

479

480   **Fig. 6.** Scatterplot of observed and simulated O3 for daytime (08:00 – 18:00 LST) in the selected

481   cites.

482

483

484

485
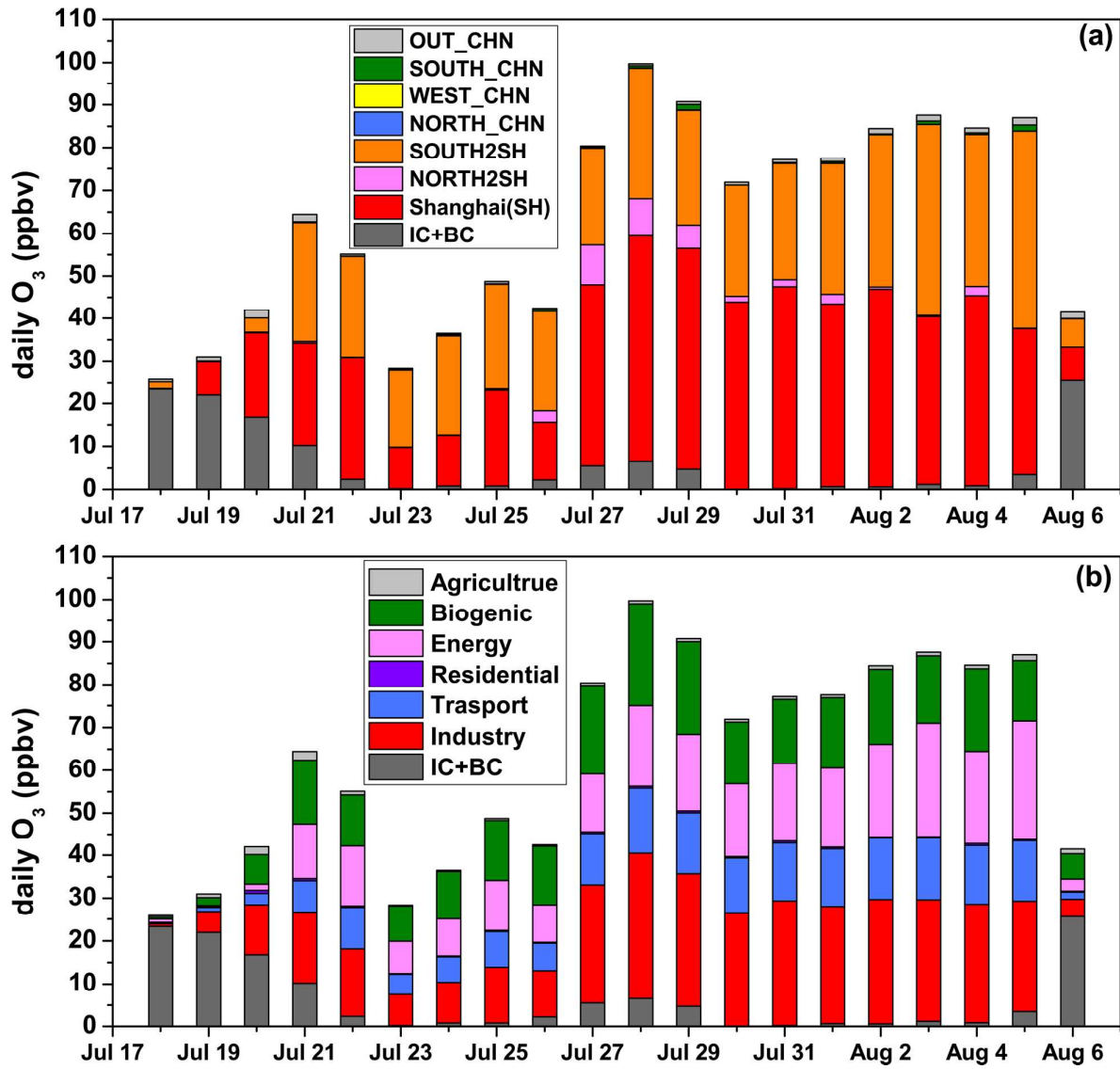
486

487

488

489

490

Fig. 7. Daytime-average (08:00 – 18:00 LST) O$_3$ contributions for Shanghai area from (a)

different source regions, and (b) different source categories for grid cells corresponding to the

493   observation sites in Shanghai. Note that the colors of the source regions are consistent with map
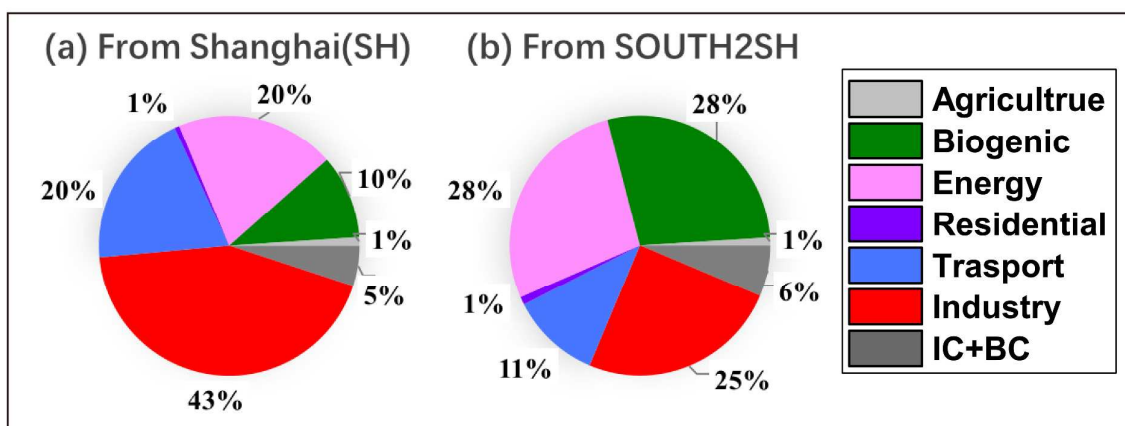
494   in Fig. 1.

495

496

497

498

499

500

501   **Fig. 8.** O$_3$ source apportionment for Shanghai area by emission category from (a) Shanghai (SH)

502   and (b) the SOUTH2SH region averaged for the episode period (daytime (08:00 – 18:00 LST)

503   from July 27 to August 5) in grid cells corresponding to the observation sites in Shanghai. Note

504   that the colors of the source categories are consistent with Fig. 7.
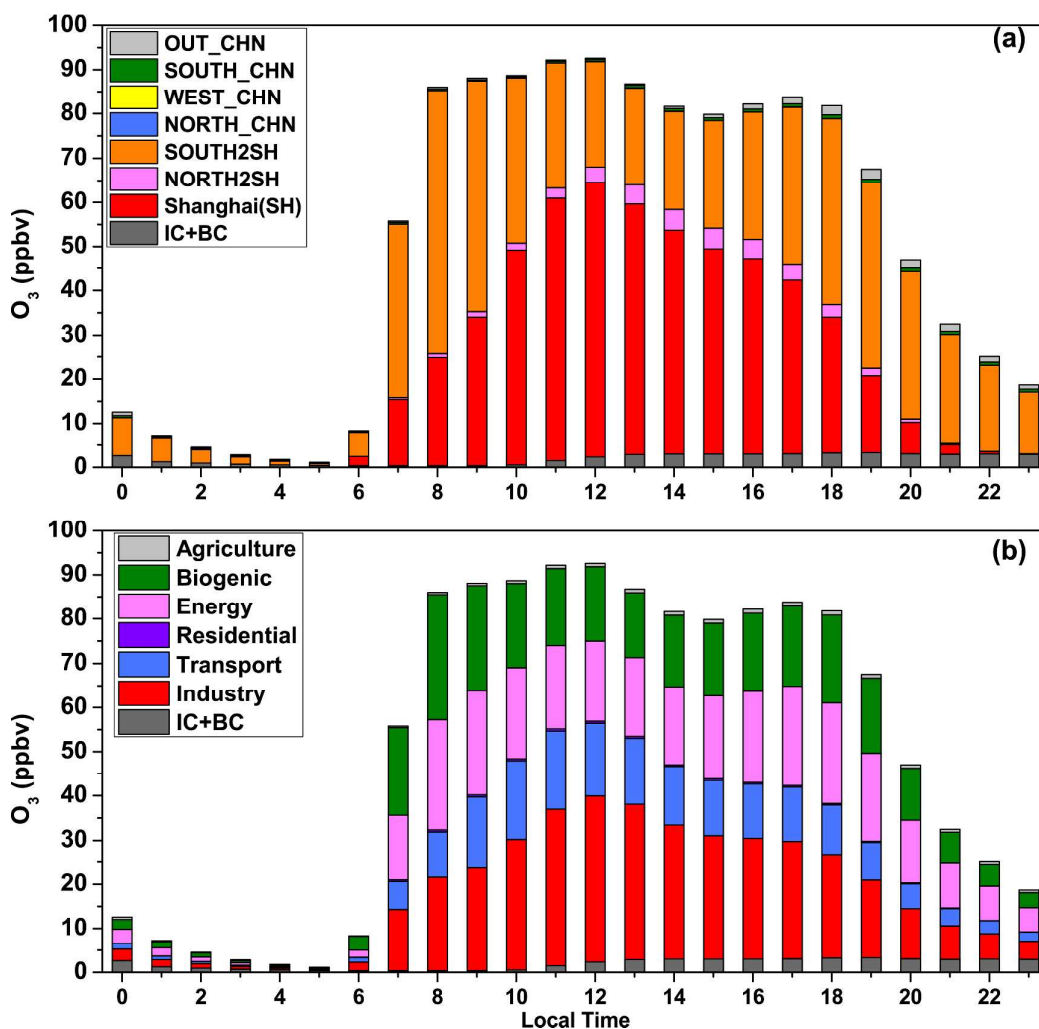
505

506

507

508

509

510

Fig. 9. Average diurnal O_3 contributions for Shanghai area from (a) different source regions, and (b) different source categories during the episode (July 27 0000 LST to August 5 2300 LST) in grid cells corresponding to the observation sites in Shanghai.
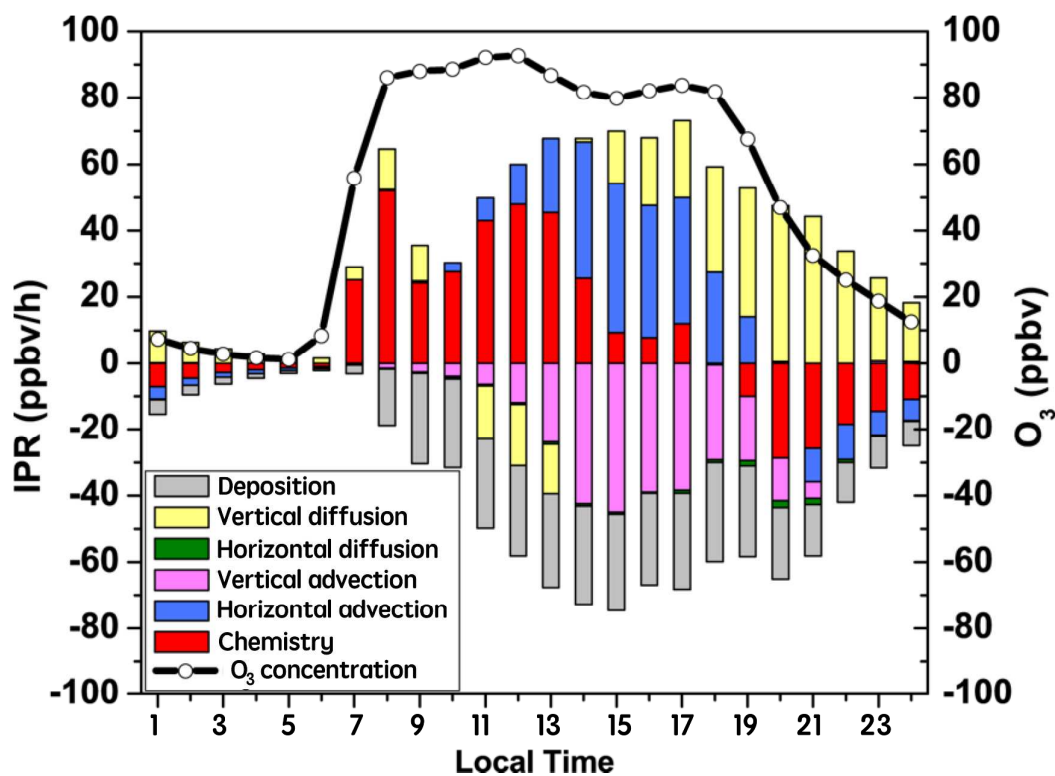
515

516

517

518

519

520

Fig. 10. Diurnal profile of O_3 concentration and the impacts of atmospheric processes on O_3 in the surface layer for Shanghai area for the episode period (July 27 0000 LST to August 5 2300 LST).